which further reduces to

$$\left|S(f,f_X,f_Y)\right| \le \sum_{m=-M'}^{M'} \sum_{n=-N'}^{N'} \left|a_{mn}(f)\right| . \tag{8B-3}$$

Therefore,

$$\max\left|S(f,f_X,f_Y)\right| = \sum_{m=-M'}^{M'} \sum_{n=-N'}^{N'} \left|a_{mn}(f)\right| . \tag{8B-4}$$

The absolute value of the real amplitude weights is required because amplitude weights can have both positive and negative values in general.

Equation (8B-4) is the absolute maximum value of $\left|S(f,f_X,f_Y)\right|$. The actual maximum value may be less than (8B-4) as indicated by (8B-3). However, if $a_{mn}(f) > 0 \ \forall \ m$ and n, then the normalization factor $S_{\max}$ for M and N odd is

$$\boxed{S_{\max} = \max\left|S(f,f_X,f_Y)\right| = \sum_{m=-M'}^{M'} \sum_{n=-N'}^{N'} a_{mn}(f)} \tag{8B-5}$$

Note that if (8B-1) is evaluated at broadside (i.e., at $f_X = 0$ and $f_Y = 0$) and if no phase weighting is done, then

$$S(f,0,0) = \sum_{m=-M'}^{M'} \sum_{n=-N'}^{N'} a_{mn}(f) \tag{8B-6}$$

and

$$\left|S(f,0,0)\right| = \left| \sum_{m=-M'}^{M'} \sum_{n=-N'}^{N'} a_{mn}(f) \right| \le \sum_{m=-M'}^{M'} \sum_{n=-N'}^{N'} \left|a_{mn}(f)\right| . \tag{8B-7}$$

If $a_{mn}(f) \ge 0 \ \forall \ m$ and n, then

$$\left|S(f,0,0)\right| = \left| \sum_{m=-M'}^{M'} \sum_{n=-N'}^{N'} a_{mn}(f) \right| = \sum_{m=-M'}^{M'} \sum_{n=-N'}^{N'} a_{mn}(f) , \tag{8B-8}$$

and by comparing (8B-5) and (8B-8),

$$\boxed{S_{\max} = \max\left|S(f,f_X,f_Y)\right| = \left|S(f,0,0)\right|} \tag{8B-9}$$

Chapter 9

Array Theory – Volume Arrays

9.1 The Far-Field Beam Pattern of a Cylindrical Array

Since a volume array is an example of a volume aperture, the far-field beam pattern (directivity function) of a volume array is given by the following three-dimensional spatial Fourier transform (see Section 1.3):

$$\begin{aligned} D(f, f_X, f_Y, f_Z) &= F_{x_A} F_{y_A} F_{z_A}\{A(f, x_A, y_A, z_A)\} \\ &= \int_{-\infty}^{\infty}\int_{-\infty}^{\infty}\int_{-\infty}^{\infty} A(f, x_A, y_A, z_A)\times \\ &\qquad \exp\left[+j2\pi(f_X x_A + f_Y y_A + f_Z z_A)\right] dx_A\, dy_A\, dz_A , \end{aligned} \tag{9.1-1}$$

where $A(f, x_A, y_A, z_A)$ is the complex frequency response (complex aperture function) of the volume array, and

$$f_X = u/\lambda = \sin\theta\cos\psi/\lambda , \tag{9.1-2}$$

$$f_Y = v/\lambda = \sin\theta\sin\psi/\lambda , \tag{9.1-3}$$

and

$$f_Z = w/\lambda = \cos\theta/\lambda \tag{9.1-4}$$

are spatial frequencies in the X, Y, and Z directions, respectively, with units of cycles per meter. Since f_X, f_Y, and f_Z can be expressed in terms of the spherical angles θ and ψ, the far-field beam pattern can ultimately be expressed as a function of frequency f and the spherical angles θ and ψ, that is, $D(f, f_X, f_Y, f_Z) \rightarrow D(f, \theta, \psi)$. We shall consider a field point to be in the far-field region of an array if the range r to the field point – as measured from the center of the array – satisfies the Fraunhofer (far-field) range criterion given by

$$r > \pi R_A^2/\lambda > 2.414 R_A , \tag{9.1-5}$$

where R_A is the maximum radial extent of the array. The units of $A(f, x_A, y_A, z_A)$ and $D(f, f_X, f_Y, f_Z)$ are summarized in Table 9.1-1 (Also see Tables 1B-1 and 1B-2).

Equation (9.1-1) can also be expressed in terms of the cylindrical coordinates (r_A, ϕ_A, z_A), as shown in Fig. 9.1-1, by noting that

Table 9.1-1 Units of the Complex Frequency Response $A(f, x_A, y_A, z_A)$ and Corresponding Far-Field Beam Pattern $D(f, f_X, f_Y, f_Z)$ for a Volume Array

Volume Array	$A(f, x_A, y_A, z_A)$	$D(f, f_X, f_Y, f_Z)$
active (transmit)	$\left(\left(\mathrm{m}^3/\mathrm{sec}\right)/\mathrm{V}\right)/\mathrm{m}^3$	$\left(\mathrm{m}^3/\mathrm{sec}\right)/\mathrm{V}$
passive (receive)	$\left(\mathrm{V}/\left(\mathrm{m}^2/\mathrm{sec}\right)\right)/\mathrm{m}^3$	$\mathrm{V}/\left(\mathrm{m}^2/\mathrm{sec}\right)$

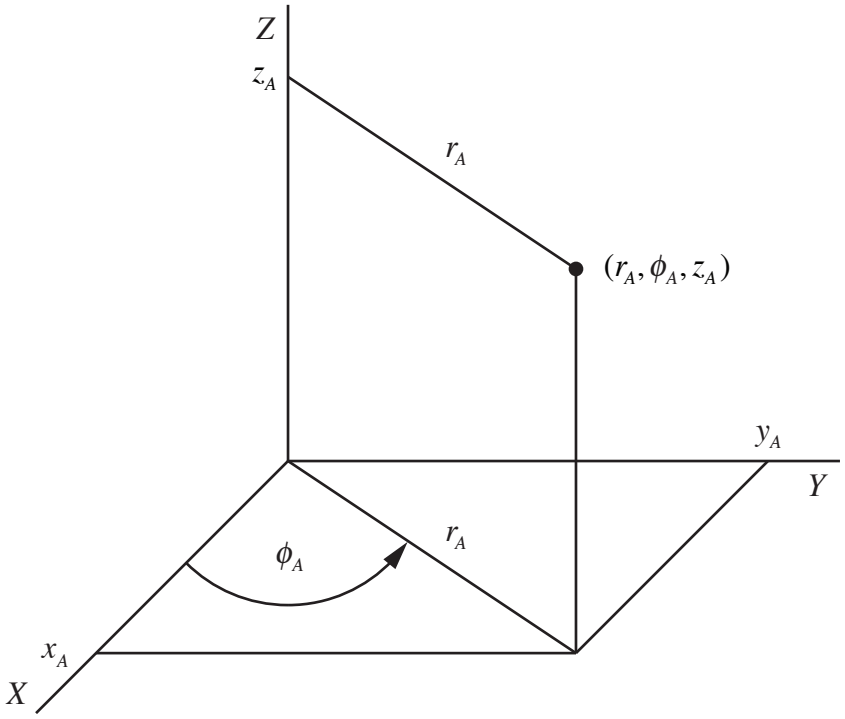

Figure 9.1-1 The cylindrical coordinates (r_A, ϕ_A, z_A).

$$x_A = r_A \cos\phi_A \,, \tag{9.1-6}$$

$$y_A = r_A \sin\phi_A \,, \tag{9.1-7}$$

$$z_A = z_A \,, \tag{9.1-8}$$

$$dx_A\, dy_A\, dz_A \to r_A\, dr_A\, d\phi_A\, dz_A \,, \tag{9.1-9}$$

and

$$A(f, x_A, y_A, z_A) = A(f, r_A \cos\phi_A, r_A \sin\phi_A, z_A) \to A(f, r_A, \phi_A, z_A) \,. \tag{9.1-10}$$

Substituting (9.1-2) through (9.1-4), and (9.1-6) through (9.1-10) into (9.1-1), and using the trigonometric identity

$$\cos(\alpha-\beta)=\cos\alpha\cos\beta+\sin\alpha\sin\beta\,, \tag{9.1-11}$$

yields

$$D(f,\theta,\psi)=\int_{-\infty}^{\infty}\int_{0}^{2\pi}\int_{0}^{\infty}A(f,r_A,\phi_A,z_A)\times \exp\left\{+j\frac{2\pi}{\lambda}\left[r_A\sin\theta\cos(\psi-\phi_A)+z_A\cos\theta\right]\right\}r_A\,dr_A\,d\phi_A\,dz_A \tag{9.1-12}$$

Equation (9.1-12) shall be used to derive the far-field beam pattern of a cylindrical array of omnidirectional point-elements. A cylindrical array is an example of a *conformal array*. A conformal array is an array of elements that lie on a *curved* surface. In other words, the array conforms to the shape of the curved surface.

Consider an array of identical, equally-spaced, complex-weighted, omnidirectional point-elements lying on the surface of a cylinder with radius a meters and length L meters (see Fig. 9.1-2). The maximum radial extent of the cylindrical array is

$$R_A=\sqrt{(L/2)^2+a^2}\,. \tag{9.1-13}$$

Any single vertical column of elements or any set of two or more adjacent vertical columns of elements (linear arrays parallel to the Z axis) is known as a *stave*. Since an impulse function is used as a mathematical model for an omnidirectional point-source in acoustic wave propagation theory, the mathematical model that we shall use for the complex frequency response of an omnidirectional point-element lying on the surface of a cylinder is given by

$$e(f,r_A-r_0,\phi_A-\phi_0,z_A-z_0)=\mathcal{S}(f)\frac{\delta(r_A-r_0)}{r_A}\delta(\phi_A-\phi_0)\delta(z_A-z_0)\,, \tag{9.1-14}$$

where $\mathcal{S}(f)$ is the complex, *element sensitivity function*, and (r_0,ϕ_0,z_0) are the cylindrical coordinates of the center of the element. If the point-element is used in the active mode as a transmitter, then the element sensitivity function $\mathcal{S}(f)$ is referred to as the *transmitter sensitivity function* with units of $\left(\mathrm{m}^3/\mathrm{sec}\right)\big/\mathrm{V}$ (see Appendix 6B). If the point-element is used in the passive mode as a receiver, then

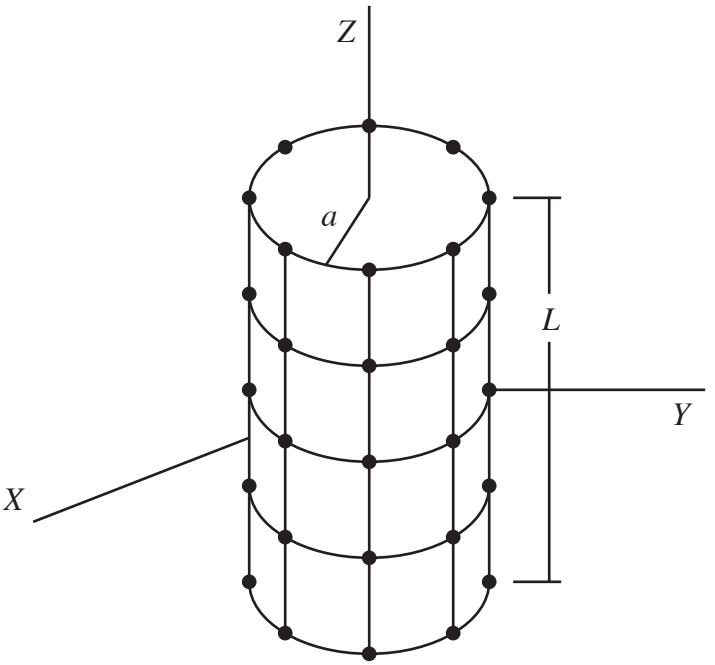

Figure 9.1-2 Cylindrical array of identical, equally-spaced, omnidirectional point-elements.

$\mathcal{S}(f)$ is referred to as the *receiver sensitivity function* with units of $\mathrm{V}/\left(\mathrm{m}^2/\mathrm{sec}\right)$ (see Appendix 6B). Note that

$$\int_{-\infty}^{\infty}\int_{0}^{2\pi}\int_{0}^{\infty} e(f, r_A - r_0, \phi_A - \phi_0, z_A - z_0)\, r_A\, dr_A\, d\phi_A\, dz_A = \mathcal{S}(f)\int_{0}^{\infty}\delta(r_A - r_0)\, dr_A \times \int_{0}^{2\pi}\delta(\phi_A - \phi_0)\, d\phi_A \times \int_{-\infty}^{\infty}\delta(z_A - z_0)\, dz_A = \mathcal{S}(f). \tag{9.1-15}$$

The impulse function $\delta(r_A - r_0)$ has units of inverse meters, $\delta(\phi_A - \phi_0)$ has units of inverse radians, and $\delta(z_A - z_0)$ has units of inverse meters. The units of $\mathcal{S}(f)$ are summarized in Table 9.1-2.

Therefore, with the use of (9.1-14) and the principle of superposition, the complex frequency response (complex aperture function) of the cylindrical array shown in Fig. 9.1-2 can be expressed as the sum of the complex-weighted frequency responses of all the elements in the array as follows:

Table 9.1-2 Units of the Element Sensitivity Function $\mathcal{S}(f)$

Omnidirectional Point-Element	$\mathcal{S}(f)$
active (transmit)	$\left(\mathrm{m}^3/\mathrm{sec}\right)/\mathrm{V}$
passive (receive)	$\mathrm{V}/\left(\mathrm{m}^2/\mathrm{sec}\right)$

$$A(f, r_A, \phi_A, z_A) = \mathcal{S}(f)\frac{\delta(r_A - a)}{r_A}\sum_{m=1}^{M}\sum_{n=-N'}^{N'} c_{mn}(f)\delta(\phi_A - \phi_m)\delta(z_A - z_n)\,, \tag{9.1-16}$$

where M is the total number (even or odd) of omnidirectional point-elements per circular array,

$$N' = (N-1)/2\,, \tag{9.1-17}$$

N is the total *odd* number of circular arrays,

$$\boxed{c_{mn}(f) = a_{mn}(f)\exp[+j\theta_{mn}(f)]} \tag{9.1-18}$$

is the frequency-dependent, *complex weight* associated with element (m,n), where $a_{mn}(f)$ is a real, frequency-dependent, *dimensionless*, amplitude weight, and $\theta_{mn}(f)$ is a real, frequency-dependent, phase weight in radians, and (a, ϕ_m, z_n) are the cylindrical coordinates of the center of element (m,n). Complex weights are implemented by using digital signal processing (digital beamforming) (see Section 6.4). The complex weights are used to control the complex frequency response of the array and, thus, the array's far-field beam pattern via amplitude and phase weighting. Since the elements are equally spaced in the ϕ and Z directions,

$$\phi_m = (m-1)\Delta\phi\,, \tag{9.1-19}$$

where

$$\Delta\phi = 360°/M\,, \tag{9.1-20}$$

and

$$z_n = nd_Z\,, \tag{9.1-21}$$

where the interelement spacing in the Z direction (in meters) is given by

$$d_Z = \frac{L}{N-1}, \quad N \neq 1. \tag{9.1-22}$$

Substituting (9.1-16) into (9.1-12) yields the following expression for the far-field beam pattern of a cylindrical array of identical, equally-spaced, complex-weighted, omnidirectional point-elements:

$$D(f,\theta,\psi) = \mathcal{S}(f)\sum_{m=1}^{M}\sum_{n=-N'}^{N'} c_{mn}(f)\exp\left[+j\frac{2\pi a}{\lambda}\sin\theta\cos(\psi-\phi_m)\right]\times \exp\left[+j\frac{2\pi}{\lambda}z_n\cos\theta\right] \tag{9.1-23}$$

where $\mathcal{S}(f)$ is the complex, element sensitivity function, and the double summation is the dimensionless array factor. If one or more elements in the array are broken (not transmitting and/or receiving), set $c_{mn}(f) = 0$ for those elements. Similarly, if only one stave is in operation at any given instant of time, set $c_{mn}(f) = 0$ for those elements not in operation.

If the number of circular arrays $N = 1$, then $N' = 0$ [see (9.1-17)] and, as a result, $n = 0$. And since $z_0 = 0$ [see (9.1-21)], (9.1-23) reduces to

$$D(f,\theta,\psi) = \mathcal{S}(f)\sum_{m=1}^{M} c_m(f)\exp\left[+j\frac{2\pi a}{\lambda}\sin\theta\cos(\psi-\phi_m)\right]. \tag{9.1-24}$$

Equation (9.1-24) is the far-field beam pattern of a single circular array with radius a meters lying in the XY plane [see (8.1-92)].

If the complex weights are separable, then

$$c_{mn}(f) = c_m(f)w_n(f), \tag{9.1-25}$$

where

$$c_m(f) = a_m(f)\exp[+j\theta_m(f)] \tag{9.1-26}$$

is the frequency-dependent, complex weight in the ϕ direction, and

$$w_n(f) = b_n(f)\exp[+j\phi_n(f)] \tag{9.1-27}$$

is the frequency-dependent, complex weight in the Z direction, where $a_m(f)$ and $b_n(f)$ are real, frequency-dependent, dimensionless, amplitude weights, and

$\theta_m(f)$ and $\phi_n(f)$ are real, frequency-dependent, phase weights in radians. Substituting (9.1-25) into (9.1-23) yields

$$\boxed{D(f,\theta,\psi) = \mathcal{S}(f)S_\phi(f,\theta,\psi)S_Z(f,\theta,\psi)} \tag{9.1-28}$$

where

$$\boxed{S_\phi(f,\theta,\psi) = \sum_{m=1}^{M} c_m(f)\exp\left[+j\frac{2\pi a}{\lambda}\sin\theta\cos(\psi-\phi_m)\right]} \tag{9.1-29}$$

and

$$\boxed{S_Z(f,\theta,\psi) = \sum_{n=-N'}^{N'} w_n(f)\exp\left[+j\frac{2\pi}{\lambda}z_n\cos\theta\right]} \tag{9.1-30}$$

are dimensionless array factors. Since

$$\cos(\psi-\phi_m) = \cos\psi\cos\phi_m + \sin\psi\sin\phi_m\,, \tag{9.1-31}$$

(9.1-29) can be rewritten as follows:

$$\boxed{S_\phi(f,\theta,\psi) = \sum_{m=1}^{M} c_m(f)\exp\left[+j\frac{2\pi}{\lambda}(x_m\sin\theta\cos\psi + y_m\sin\theta\sin\psi)\right]} \tag{9.1-32}$$

where

$$x_m = a\cos\phi_m \tag{9.1-33}$$

and

$$y_m = a\sin\phi_m \tag{9.1-34}$$

are the rectangular coordinates of element m in a circular array with radius a meters, and ϕ_m is given by (9.1-19).

9.1.1 The Phased Array – Beam Steering

Beam steering can be accomplished by operating staves in a clockwise or counterclockwise fashion. This is known as *scanning*. When a particular stave is in operation, the far-field beam pattern of the stave can be steered to $\theta = \theta'$ and $\psi = \psi'$ by using separable complex weights with the following phase weights:

$$\theta_m(f) = -\frac{2\pi}{\lambda}(x_m \sin\theta' \cos\psi' + y_m \sin\theta' \sin\psi'), \qquad m = 1, 2, \ldots, M \tag{9.1-35}$$

where x_m and y_m are given by (9.1-33) and (9.1-34), respectively, and

$$\phi_n(f) = -\frac{2\pi}{\lambda} z_n \cos\theta', \qquad n = -N', \ldots, 0, \ldots, N' \tag{9.1-36}$$

where z_n is given by (9.1-21). Substituting (9.1-26) and (9.1-35) into (9.1-32), and (9.1-27) and (9.1-36) into (9.1-30) yields

$$S_\phi(f, \theta, \psi) = \sum_{m=1}^{M} a_m(f) \exp\left[+j\frac{2\pi}{\lambda}(\sin\theta\cos\psi - \sin\theta'\cos\psi')x_m\right] \times \exp\left[+j\frac{2\pi}{\lambda}(\sin\theta\sin\psi - \sin\theta'\sin\psi')y_m\right] \tag{9.1-37}$$

and

$$S_Z(f, \theta, \psi) = \sum_{n=-N'}^{N'} b_n(f) \exp\left[+j\frac{2\pi}{\lambda}(\cos\theta - \cos\theta')z_n\right] \tag{9.1-38}$$

respectively. Therefore, the far-field beam pattern of a particular stave of the cylindrical array when beam steering is done is obtained by substituting (9.1-37) and (9.1-38) into (9.1-28), and by setting $a_m(f) = 0$ in (9.1-37) for those elements not in operation. By operating two or more staves at the same time and using *parallel signal processing*, multiple beams with multiple "look directions" can be formed *simultaneously*.

Finally, note that a phase weight $\theta_{mn}(f)$ in radians is equivalent to a *time delay* τ'_{mn} in seconds, that is,

$$\theta_{mn}(f) \triangleq -2\pi f \tau'_{mn}, \tag{9.1-39}$$

or

$$\tau'_{mn} = -\theta_{mn}(f)/(2\pi f). \tag{9.1-40}$$

In our case,

$$\theta_{mn}(f) = \theta_m(f) + \phi_n(f), \tag{9.1-41}$$

where $\theta_m(f)$ and $\phi_n(f)$ are given by (9.1-35) and (9.1-36), respectively. Substituting (9.1-41), (9.1-35), and (9.1-36) into (9.1-40) yields

$$\tau'_{mn} = \frac{u'}{c}x_m + \frac{v'}{c}y_m + \frac{w'}{c}z_n, \qquad \begin{matrix} m = 1, 2, \ldots, M \\ n = -N', \ldots, 0, \ldots, N' \end{matrix} \tag{9.1-42}$$

where $c = f\lambda$, and

$$u' = \sin\theta' \cos\psi', \tag{9.1-43}$$

$$v' = \sin\theta' \sin\psi', \tag{9.1-44}$$

and

$$w' = \cos\theta'. \tag{9.1-45}$$

Example 9.1-1

Let $M = 30$, where M is the total number of omnidirectional point-elements per circular array. As a result, the angular spacing in the ϕ direction $\Delta\phi = 12°$ [see (9.1-20)], and angle $\phi_m = (m-1)12°$, $m = 1, 2, \ldots, 30$ [see (9.1-19)]. Also, let a single stave be composed of five adjacent vertical columns of elements, and let the range of values for index m for stave 1 be $m = 1, 2, 3, 4, 5$; for stave 2, $m = 2, 3, 4, 5, 6$; … ; for stave 26, $m = 26, 27, 28, 29, 30$; for stave 27, $m = 27, 28, 29, 30, 1$; … ; and for stave 30, $m = 30, 1, 2, 3, 4$. Therefore, for stave 1, $\phi_1 = 0°$, $\phi_2 = 12°$, $\phi_3 = 24°$, $\phi_4 = 36°$, $\phi_5 = 48°$, beam-steer angle $\psi' = \phi_3 = 24°$, and amplitude weight $a_m(f) = 0$ for $m = 6, 7, \ldots, 30$; for stave 2, $\phi_2 = 12°$, $\phi_3 = 24°$, $\phi_4 = 36°$, $\phi_5 = 48°$, $\phi_6 = 60°$, $\psi' = \phi_4 = 36°$, and $a_m(f) = 0$ for $m = 1$ and $m = 7, 8, \ldots, 30$; etc. Note that for stave 29, $\psi' = \phi_1 = 0°$; and for stave 30, $\psi' = \phi_2 = 12°$. If stave 2 is currently in operation, then substituting (9.1-33) and (9.1-34) into (9.1-37), and summing over index m from 2 to 6 yields

$$S_\phi(f, \theta, \psi) = \sum_{m=2}^{6} a_m(f) \exp\left[+j\frac{2\pi a}{\lambda}(\sin\theta\cos\psi - \sin\theta'\cos\psi')\cos\phi_m\right] \times \exp\left[+j\frac{2\pi a}{\lambda}(\sin\theta\sin\psi - \sin\theta'\sin\psi')\sin\phi_m\right] \tag{9.1-46}$$

where $\phi_2 = 12°$, $\phi_3 = 24°$, $\phi_4 = 36°$, $\phi_5 = 48°$, $\phi_6 = 60°$, and $\psi' = \phi_4 = 36°$. Note that ψ' does not have to be equal to ϕ_4. The array factor $S_Z(f, \theta, \psi)$ given by (9.1-38) remains unchanged. However, by substituting (9.1-21) and (9.1-22) into (9.1-38), it can be rewritten as

$$S_Z(f, \theta, \psi) = \sum_{n=-N'}^{N'} b_n(f) \exp\left[+j2\pi \frac{L}{\lambda}(\cos\theta - \cos\theta')\frac{n}{N-1}\right]. \quad (9.1\text{-}47)$$

Substituting (9.1-46) and (9.1-47) into (9.1-28) yields the far-field beam pattern of stave 2. At $\theta = \theta'$ and $\psi = \psi'$,

$$\begin{aligned} D(f, \theta', \psi') &= \mathcal{S}(f) S_\phi(f, \theta', \psi') S_Z(f, \theta', \psi') \\ &= \mathcal{S}(f) \sum_{m=2}^{6} a_m(f) \sum_{n=-N'}^{N'} b_n(f). \end{aligned} \quad (9.1\text{-}48)$$

If both sets of amplitude weights are rectangular amplitude weights, that is, if $a_m(f) = 1$, $m = 2, 3, \ldots, 6$, and $b_n(f) = 1 \ \forall \ n$, then

$$D(f, \theta', \psi') = 5N\mathcal{S}(f), \quad (9.1\text{-}49)$$

where N is the total odd number of circular arrays (or elements in a linear array parallel to the Z axis).

Figure 9.1-3 is a polar plot, as a function of the azimuthal (bearing) angle ψ, of the magnitude of the normalized, horizontal, far-field beam pattern of stave 2 in the first quadrant for $M = 30$, $N = 9$, rectangular amplitude weights, $ka = 2\pi a/\lambda = 15$, $L/\lambda = 4$, and for (a) no beam steering, and for beam-steer angles (b) $\theta' = 90°$ and $\psi' = \phi_4 = 36°$, and (c) $\theta' = 90°$ and $\psi' = 30°$. Note that the axis of the mainlobe in Fig. 9.1-3 (a) is at $\psi = \phi_4 = 36°$ even though no beam steering was done. However, as can be seen in Fig. 9.1-3 (b), when beam steering is done using $\theta' = 90°$ and $\psi' = \phi_4 = 36°$, the mainlobe in Fig. 9.1-3 (b) is well defined compared to the mainlobe in Fig. 9.1-3 (a), and the sidelobes in Fig. 9.1-3 (b) are lower than the sidelobes in Fig. 9.1-3 (a). Figure 9.1-4 is a polar plot, as a function of the vertical angle θ, of the magnitude of the normalized, vertical, far-field beam pattern of stave 2 in the plane with bearing angle $\psi = \psi'$ for $M = 30$, $N = 9$, rectangular amplitude weights, $ka = 2\pi a/\lambda = 15$, $L/\lambda = 4$, and for beam-steer angles (a) $\theta' = 135°$ and $\psi' = \phi_4 = 36°$, and (b) $\theta' = 135°$ and $\psi' = 30°$. ■

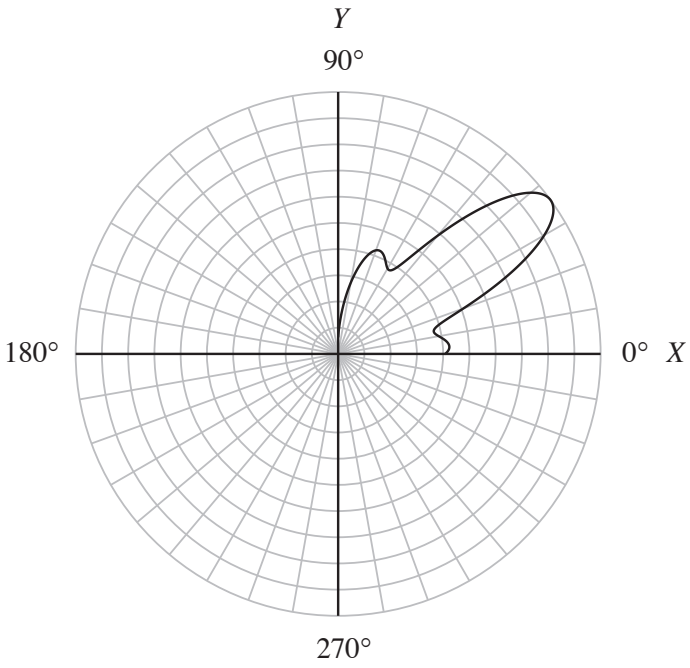

(a)

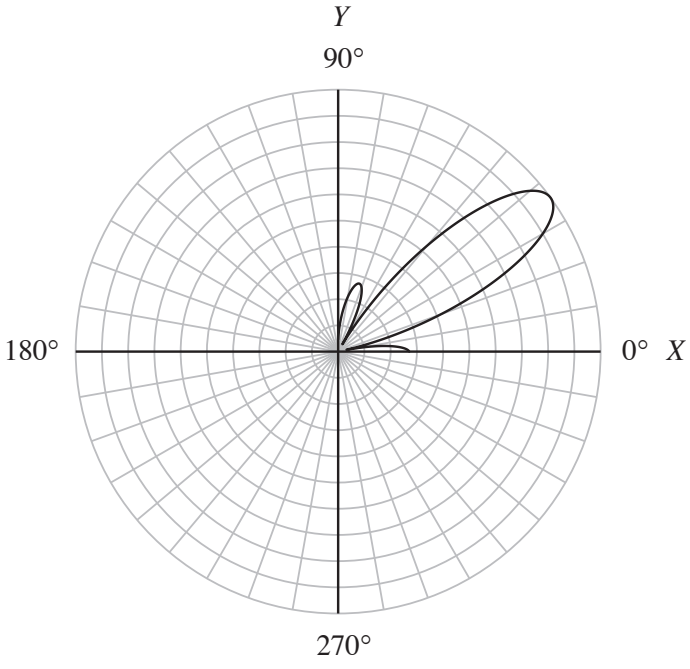

(b)

Figure 9.1-3 Polar plot, as a function of the azimuthal (bearing) angle ψ, of the magnitude of the normalized, horizontal, far-field beam pattern of stave 2 in the first quadrant for the cylindrical array discussed in Example 9.1-1 for (a) no beam steering, and for beam-steer angles (b) $\theta' = 90°$ and $\psi' = \phi_4 = 36°$, and (c) $\theta' = 90°$ and $\psi' = 30°$.

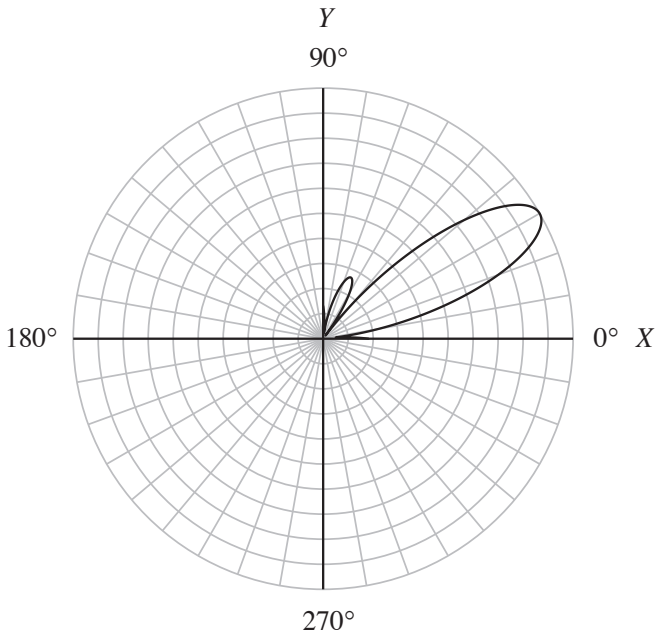

(c)

Figure 9.1-3 *continued*.

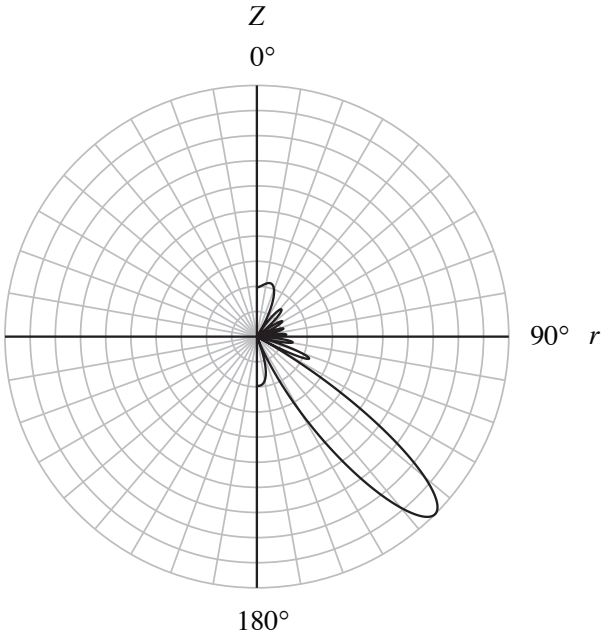

(a)

Figure 9.1-4 Polar plot, as a function of the vertical angle θ, of the magnitude of the normalized, vertical, far-field beam pattern of stave 2 in the plane with bearing angle $\psi = \psi'$ for the cylindrical array discussed in Example 9.1-1 for beam-steer angles (a) $\theta' = 135°$ and $\psi' = \phi_4 = 36°$, and (b) $\theta' = 135°$ and $\psi' = 30°$, where r is horizontal range.

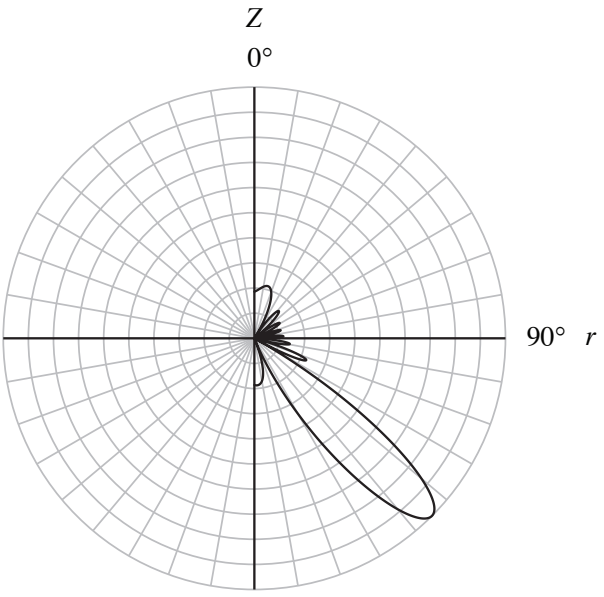

(b)

Figure 9.1-4 *continued*.

Example 9.1-2 Linear Array of Triplets

One solution to the port/starboard (left/right) ambiguity problem associated with linear arrays is a twin-line planar array (see Example 8.2-1). Another solution is a linear array of *triplets*. A single triplet is discussed in Example 8.1-7. In this example we shall consider a linear array composed of an odd number N of identical, equally-spaced, complex-weighted, triplets perpendicular to the array axis as shown in Fig. 9.1-5. Each triplet has a radius of a meters. The array shown in Fig. 9.1-5 is analogous to a cylindrical array of identical, equally-spaced, complex-weighted, omnidirectional point-elements that is lying on its side.

Since the elements (triplets) are identical, the far-field beam pattern of the array shown in Fig. 9.1-5 can be obtained by using the Product Theorem. Doing so yields

$$D(f, f_X, f_Y, f_Z) = E(f, f_X, f_Z) S_Y(f, f_Y) , \tag{9.1-50}$$

or

$$D(f, u, v, w) = E(f, u, w) S_Y(f, v) , \tag{9.1-51}$$

where $E(f, u, w)$ is the far-field beam pattern of a single triplet in the XZ plane,

$$S_Y(f, v) = \sum_{n=-N'}^{N'} w_n(f) \exp\left(+j2\pi v n d_Y / \lambda\right) \tag{9.1-52}$$

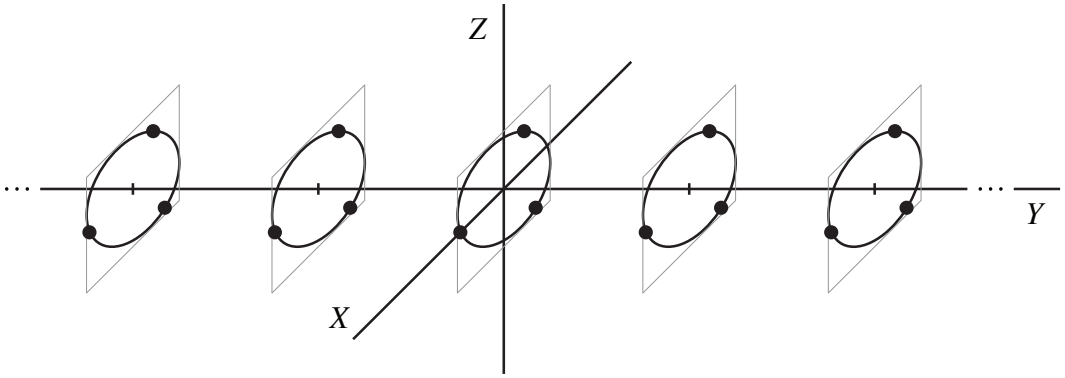

Figure 9.1-5 Linear array of identical, equally-spaced, triplets perpendicular to the array axis.

is the dimensionless array factor in the Y direction,

$$w_n(f) = b_n(f)\exp[+j\phi_n(f)] \tag{9.1-53}$$

is a frequency-dependent, complex weight associated with the nth triplet, $b_n(f)$ is a real, frequency-dependent, dimensionless, amplitude weight, $\phi_n(f)$ is a real, frequency-dependent, phase weight in radians, d_Y is the interelement spacing in meters between the triplets along the Y axis, and

$$N' = (N-1)/2\,. \tag{9.1-54}$$

Since the triplets are lying in the XZ plane, the far-field beam pattern $E(f,u,w)$ can be obtained by replacing direction cosine v in (8.1-100) with direction cosine w yielding

$$E(f,u,w) = \mathcal{S}(f)\left[c_1(f)\exp(+jkau) + c_2(f)\exp\left[-j\frac{ka}{2}\left(u-\sqrt{3}\,w\right)\right] + c_3(f)\exp\left[-j\frac{ka}{2}\left(u+\sqrt{3}\,w\right)\right]\right], \tag{9.1-55}$$

where $\mathcal{S}(f)$ is the complex, element sensitivity function of the omnidirectional point-elements in a triplet.

From Example 8.1-7, in order to create a *cardioid* (heart-shaped) beam pattern from a triplet,

$$ka = \pi/3\,, \tag{9.1-56}$$

$$c_1(f) = 2\,\mathrm{a}(f)\exp\left(-j\pi/2\right), \tag{9.1-57}$$

and

$$c_3(f) = c_2(f) = \mathrm{a}(f), \tag{9.1-58}$$

where $\mathrm{a}(f)$ is a real, frequency-dependent, dimensionless, amplitude weight. Substituting (9.1-56) through (9.1-58) into (9.1-55) yields the *unnormalized*, *cardioid*, far-field beam pattern of a triplet lying in the XZ plane:

$$\boxed{E(f,u,w) = 2\,\mathrm{a}(f)\mathcal{S}(f)\exp\left(+j\frac{\pi}{3}u\right)\left[\exp\left(-j\frac{\pi}{2}u\right)\cos\left(\frac{\sqrt{3}}{6}\pi w\right) - j\right]} \tag{9.1-59}$$

In order to do beam steering, let the phase weight

$$\phi_n(f) = -2\pi v' n d_Y/\lambda, \tag{9.1-60}$$

where

$$v' = \sin\theta' \sin\psi'. \tag{9.1-61}$$

Substituting (9.1-53) and (9.1-60) into (9.1-52) yields

$$S_Y(f,v) = \sum_{n=-N'}^{N'} b_n(f)\exp\left[+j2\pi(v-v')n d_Y/\lambda\right]. \tag{9.1-62}$$

Substituting (9.1-59) and (9.1-62) into (9.1-51) yields

$$D(f,u,v,w) = 2\,\mathrm{a}(f)\mathcal{S}(f)\exp\left(+j\frac{\pi}{3}u\right)\left[\exp\left(-j\frac{\pi}{2}u\right)\cos\left(\frac{\sqrt{3}}{6}\pi w\right) - j\right]\times$$
$$\sum_{n=-N'}^{N'} b_n(f)\exp\left[+j2\pi(v-v')n d_Y/\lambda\right], \tag{9.1-63}$$

or

$$\boxed{\begin{aligned} D(f,\theta,\psi) = {} & 2\,\mathrm{a}(f)\mathcal{S}(f)\exp\left(+j\frac{\pi}{3}\sin\theta\cos\psi\right)\times \\ & \left[\exp\left(-j\frac{\pi}{2}\sin\theta\cos\psi\right)\cos\left(\frac{\sqrt{3}}{6}\pi\cos\theta\right) - j\right]\times \\ & \sum_{n=-N'}^{N'} b_n(f)\exp\left[+j2\pi(\sin\theta\sin\psi - \sin\theta'\sin\psi')n d_Y/\lambda\right] \end{aligned}} \tag{9.1-64}$$

Equation (9.1-64) is the *unnormalized*, far-field beam pattern of a linear array of triplets with magnitude

$$\left|D(f,\theta,\psi)\right| = 2\left|\mathrm{a}(f)\right|\left|\mathcal{S}(f)\right|\left|\exp\left(-j\frac{\pi}{2}\sin\theta\cos\psi\right)\cos\left(\frac{\sqrt{3}}{6}\pi\cos\theta\right)-j\right|\times$$
$$\left|\sum_{n=-N'}^{N'} b_n(f)\exp\left[+j2\pi(\sin\theta\sin\psi-\sin\theta'\sin\psi')nd_Y/\lambda\right]\right|. \tag{9.1-65}$$

Setting $\theta = 90°$ and $\theta' = 90°$ in (9.1-65) yields

$$\left|D(f,90°,\psi)\right| = 2\left|\mathrm{a}(f)\right|\left|\mathcal{S}(f)\right|\left|\exp\left(-j\frac{\pi}{2}\cos\psi\right)-j\right|\times$$
$$\left|\sum_{n=-N'}^{N'} b_n(f)\exp\left[+j2\pi(\sin\psi-\sin\psi')nd_Y/\lambda\right]\right|, \tag{9.1-66}$$

which is the magnitude of the unnormalized, *horizontal*, far-field beam pattern in the XY plane. Figure 9.1-6 is a plot of (9.1-66) for $\left|\mathrm{a}(f)\right| = 1$ and $\left|\mathcal{S}(f)\right| = 1$. Figure 9.1-6 (b) shows that the magnitude of the main lobe at $\psi = 45°$ is less than the maximum value at $\psi = 0°$ (broadside) shown in Fig. 9.1-6 (a). If the array is towed in the positive Y direction, then $\psi = 0°$ is broadside on the starboard (right) side of the array, and $\psi = 180°$ is broadside on the port (left) side of the array.

If the complex weight

$$c_1(f) = 2\,\mathrm{a}(f)\exp\left(+j\pi/2\right), \tag{9.1-67}$$

then the *unnormalized*, *cardioid*, far-field beam pattern of a triplet lying in the XZ plane is given by (see Example 8.1-7)

$$\boxed{E(f,u,w) = 2\,\mathrm{a}(f)\mathcal{S}(f)\exp\left(+j\frac{\pi}{3}u\right)\left[\exp\left(-j\frac{\pi}{2}u\right)\cos\left(\frac{\sqrt{3}}{6}\pi w\right)+j\right]} \tag{9.1-68}$$

and the *unnormalized*, far-field beam pattern of a linear array of triplets is given by

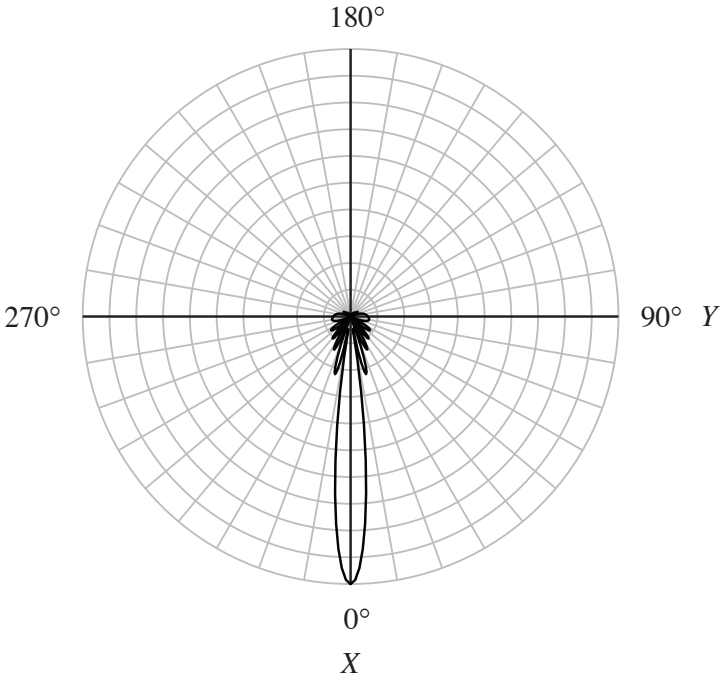

(a)

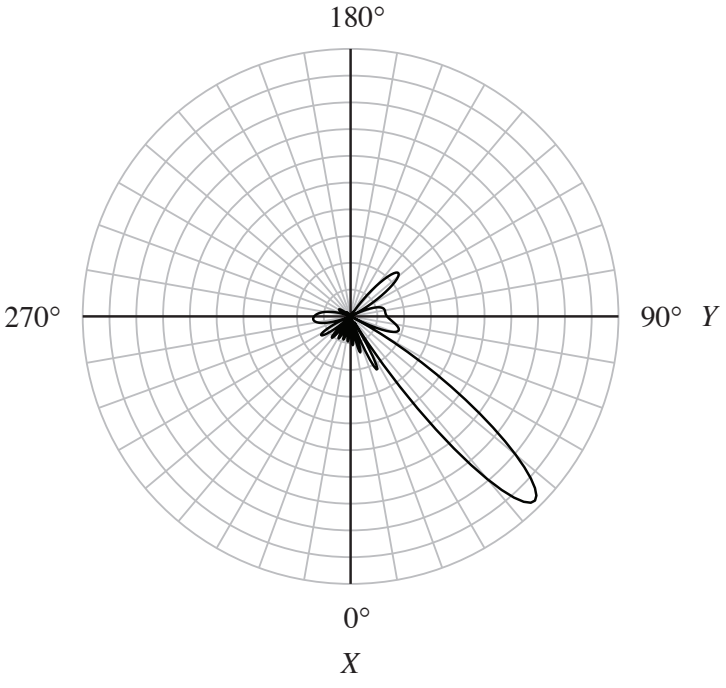

(b)

Figure 9.1-6 Polar plot, as a function of the azimuthal (bearing) angle ψ, of the magnitude of the unnormalized, horizontal, far-field beam pattern of a linear array of triplets given by (9.1-66) for $N = 11$, $d_Y/\lambda = 0.5$, rectangular amplitude weights, and beam-steer angles (a) $\psi' = 0°$ (broadside) and (b) $\psi' = 45°$.

$$D(f,\theta,\psi)=2\,\mathrm{a}(f)\,\boldsymbol{\mathcal{S}}(f)\exp\left(+j\frac{\pi}{3}\sin\theta\cos\psi\right)\times \left[\exp\left(-j\frac{\pi}{2}\sin\theta\cos\psi\right)\cos\left(\frac{\sqrt{3}}{6}\pi\cos\theta\right)+j\right]\times \sum_{n=-N'}^{N'} b_n(f)\exp\left[+j2\pi(\sin\theta\sin\psi-\sin\theta'\sin\psi')nd_Y/\lambda\right] \tag{9.1-69}$$

with magnitude

$$\left|D(f,\theta,\psi)\right|=2\left|\mathrm{a}(f)\right|\left|\boldsymbol{\mathcal{S}}(f)\right|\left|\exp\left(-j\frac{\pi}{2}\sin\theta\cos\psi\right)\cos\left(\frac{\sqrt{3}}{6}\pi\cos\theta\right)+j\right|\times \left|\sum_{n=-N'}^{N'} b_n(f)\exp\left[+j2\pi(\sin\theta\sin\psi-\sin\theta'\sin\psi')nd_Y/\lambda\right]\right|. \tag{9.1-70}$$

Setting $\theta=90°$ and $\theta'=90°$ in (9.1-70) yields

$$\left|D(f,90°,\psi)\right|=2\left|\mathrm{a}(f)\right|\left|\boldsymbol{\mathcal{S}}(f)\right|\left|\exp\left(-j\frac{\pi}{2}\cos\psi\right)+j\right|\times \left|\sum_{n=-N'}^{N'} b_n(f)\exp\left[+j2\pi(\sin\psi-\sin\psi')nd_Y/\lambda\right]\right|, \tag{9.1-71}$$

which is the magnitude of the unnormalized, *horizontal*, far-field beam pattern in the XY plane. Figure 9.1-7 is a plot of (9.1-71) for $\left|\mathrm{a}(f)\right|=1$ and $\left|\boldsymbol{\mathcal{S}}(f)\right|=1$. Although not very visible from the polar plot shown in Fig. 9.1-7 (b), the data shows that the magnitude of the main lobe at $\psi=210°$ is slightly less than the maximum value at $\psi=180°$ (broadside) shown in Fig. 9.1-7 (a).

Like the main lobes of the horizontal, far-field beam patterns of a twin-line planar array shown in Figs. 8.2-3 and 8.2-4, the main lobes of the horizontal, far-field beam patterns shown in Figs. 9.1-6 and 9.1-7 exist in a half-space. Compare Figs. 8.2-3 and 8.2-4 with Figs. 9.1-6 and 9.1-7, respectively. Note that the sidelobe levels are lower in Figs. 9.1-6 and 9.1-7 compared to Figs. 8.2-3 and 8.2-4. Although the horizontal beam patterns in Figs. 8.2-3 and 8.2-4 are normalized, the unnormalized, horizontal beam patterns also have their maximum values at the beam-steer angles $\psi'=45°$ and $\psi'=210°$ unlike the unnormalized, horizontal beam patterns of a linear array of triplets. ■

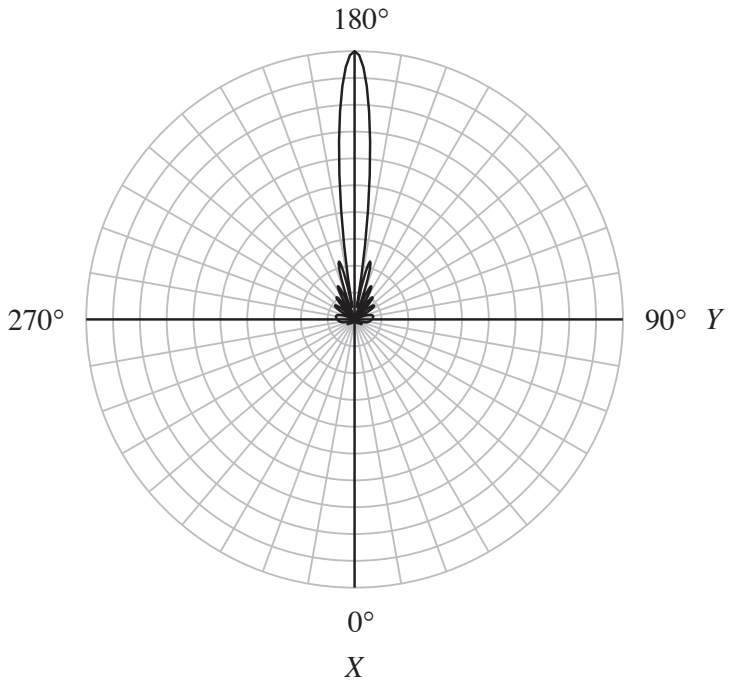

(a)

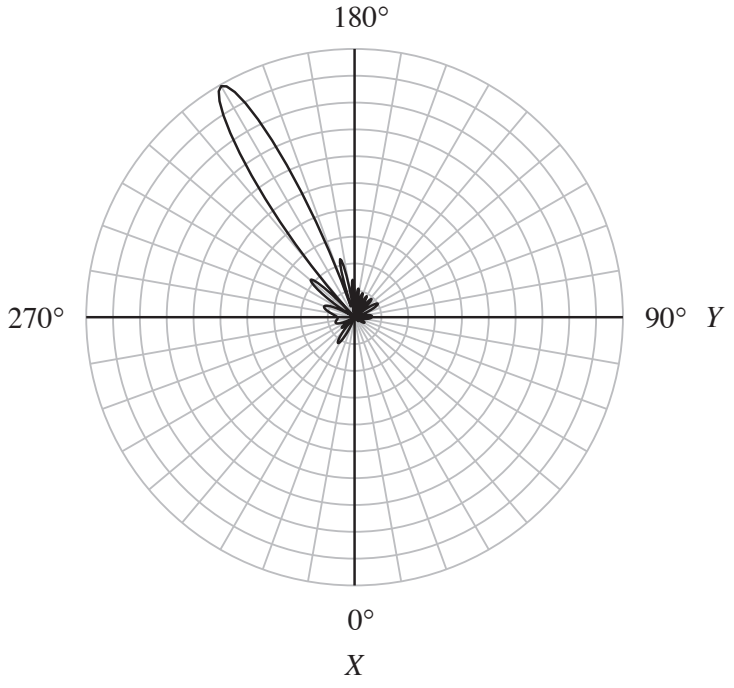

(b)

Figure 9.1-7 Polar plot, as a function of the azimuthal (bearing) angle ψ, of the magnitude of the unnormalized, horizontal, far-field beam pattern of a linear array of triplets given by (9.1-71) for $N = 11$, $d_Y/\lambda = 0.5$, rectangular amplitude weights, and beam-steer angles (a) $\psi' = 180°$ (broadside) and (b) $\psi' = 210°$.

9.2 The Far-Field Beam Pattern of a Spherical Array

Equation (9.1-1) can also be expressed in terms of the spherical coordinates (r_A, γ_A, ϕ_A), as shown in Fig. 9.2-1, by noting that

$$x_A = r_A \sin\gamma_A \cos\phi_A , \tag{9.2-1}$$

$$y_A = r_A \sin\gamma_A \sin\phi_A , \tag{9.2-2}$$

$$z_A = r_A \cos\gamma_A , \tag{9.2-3}$$

$$dx_A\, dy_A\, dz_A \rightarrow r_A^2 \sin\gamma_A\, dr_A\, d\gamma_A\, d\phi_A , \tag{9.2-4}$$

and

$$A(f, x_A, y_A, z_A) = A(f, r_A \sin\gamma_A \cos\phi_A, r_A \sin\gamma_A \sin\phi_A, r_A \cos\gamma_A) \rightarrow A(f, r_A, \gamma_A, \phi_A) . \tag{9.2-5}$$

Substituting (9.1-2) through (9.1-4), and (9.2-1) through (9.2-5) into (9.1-1), and using the trigonometric identity

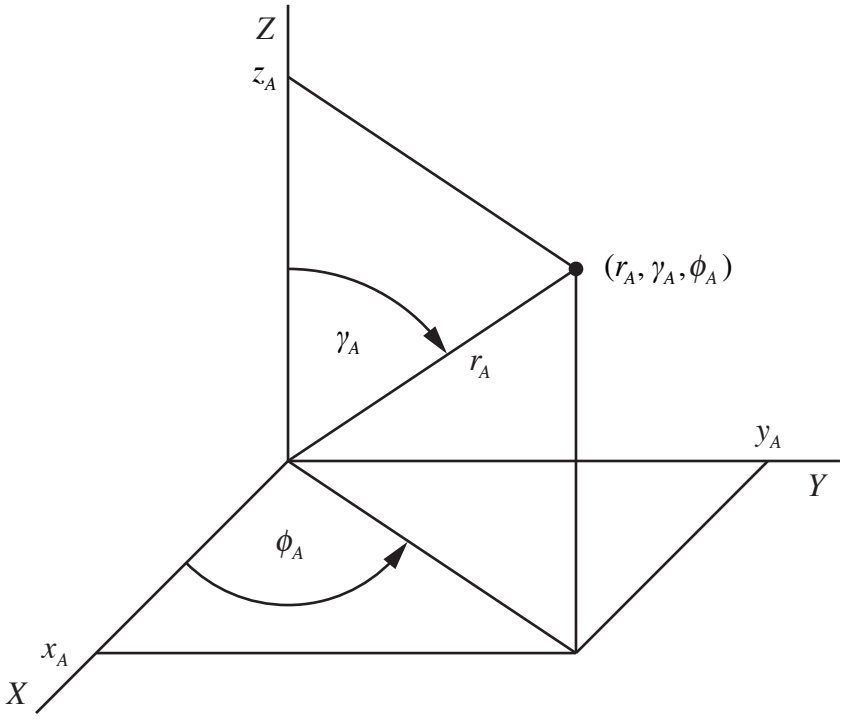

Figure 9.2-1 The spherical coordinates (r_A, γ_A, ϕ_A).

$$\cos(\alpha-\beta)=\cos\alpha\cos\beta+\sin\alpha\sin\beta\,, \tag{9.2-6}$$

yields

$$D(f,\theta,\psi)=\int_0^{2\pi}\int_0^{\pi}\int_0^{\infty}A(f,r_A,\gamma_A,\phi_A)\times \exp\left\{+j\frac{2\pi r_A}{\lambda}\left[\sin\gamma_A\sin\theta\cos(\psi-\phi_A)+\cos\gamma_A\cos\theta\right]\right\}\times r_A^2\sin\gamma_A\,dr_A\,d\gamma_A\,d\phi_A \tag{9.2-7}$$

Equation (9.2-7) shall be used to derive the far-field beam pattern of a spherical array of omnidirectional point-elements. Like the cylindrical array discussed in Section 9.1, a spherical array is another example of a conformal array.

Consider an array of identical, equally-spaced, complex-weighted, omnidirectional point-elements lying on the surface of a sphere with radius a meters (see Fig. 9.2-2). The maximum radial extent of the spherical array is $R_A=a$ meters. Analogous to a cylindrical array, let us consider a stave to be any single vertical line array of elements or any set of two or more adjacent vertical line arrays of elements running from north to south on the surface of the sphere (lines of longitude). Since an impulse function is used as a mathematical model for an omnidirectional point-source in acoustic wave propagation theory, the mathematical model that we shall use for the complex frequency response of an omnidirectional point-element lying on the surface of a sphere is given by

$$e(f,r_A-r_0,\gamma_A-\gamma_0,\phi_A-\phi_0)=\mathcal{S}(f)\frac{\delta(r_A-r_0)}{r_A^2}\frac{\delta(\gamma_A-\gamma_0)}{\sin\gamma_A}\delta(\phi_A-\phi_0)\,, \tag{9.2-8}$$

where $\mathcal{S}(f)$ is the complex, element sensitivity function (see Table 9.1-2 and Appendix 6B), and (r_0,γ_0,ϕ_0) are the spherical coordinates of the center of the element. Note that

$$\int_0^{2\pi}\int_0^{\pi}\int_0^{\infty}e(f,r_A-r_0,\gamma_A-\gamma_0,\phi_A-\phi_0)r_A^2\sin\gamma_A\,dr_A\,d\gamma_A\,d\phi_A=\mathcal{S}(f)\int_0^{\infty}\delta(r_A-r_0)dr_A\times\int_0^{\pi}\delta(\gamma_A-\gamma_0)d\gamma_A\times\int_0^{2\pi}\delta(\phi_A-\phi_0)d\phi_A=\mathcal{S}(f). \tag{9.2-9}$$

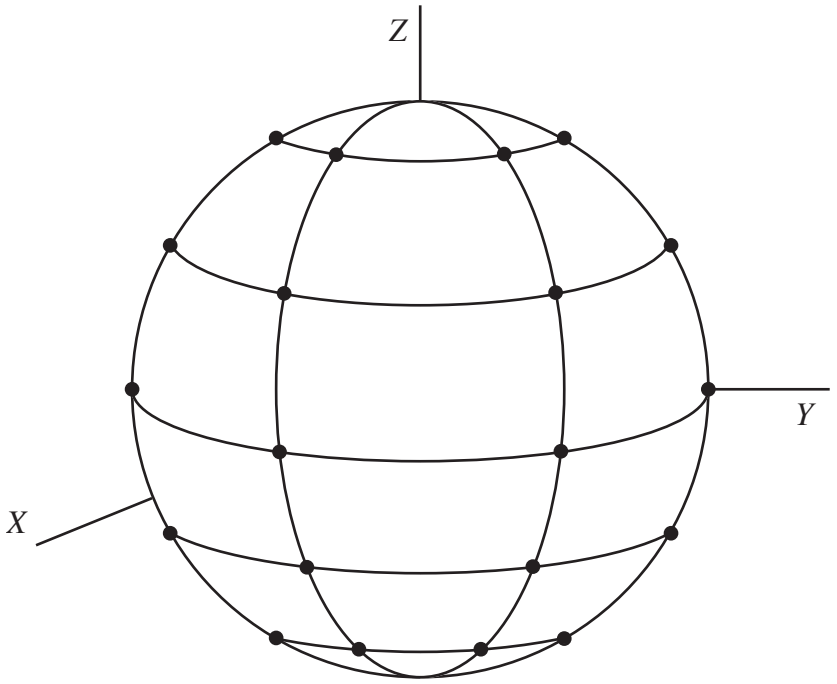

Figure 9.2-2 Spherical array of identical, equally-spaced, omnidirectional point-elements.

The impulse function $\delta(r_A - r_0)$ has units of inverse meters, and the impulse functions $\delta(\gamma_A - \gamma_0)$ and $\delta(\phi_A - \phi_0)$ have units of inverse radians.

Therefore, with the use of (9.2-8) and the principle of superposition, the complex frequency response (complex aperture function) of the spherical array shown in Fig. 9.2-2 can be expressed as the sum of the complex-weighted frequency responses of all the elements in the array as follows:

$$A(f, r_A, \gamma_A, \phi_A) = S(f) \frac{\delta(r_A - a)}{r_A^2 \sin\gamma_A} \sum_{m=1}^{M} \sum_{n=1}^{N} c_{mn}(f) \delta(\gamma_A - \gamma_m) \delta(\phi_A - \phi_n), \tag{9.2-10}$$

where M is the total *odd* number of circular arrays, N is the total number (even or odd) of omnidirectional point-elements per circular array,

$$c_{mn}(f) = a_{mn}(f) \exp[+j\theta_{mn}(f)] \tag{9.2-11}$$

is the frequency-dependent, complex weight associated with element (m,n), where $a_{mn}(f)$ is a real, frequency-dependent, dimensionless, amplitude weight, and $\theta_{mn}(f)$ is a real, frequency-dependent, phase weight in radians, and

(a, γ_m, ϕ_n) are the spherical coordinates of the center of element (m,n). Complex weights are implemented by using digital signal processing (digital beamforming) (see Section 6.4). The complex weights are used to control the complex frequency response of the array and, thus, the array's far-field beam pattern via amplitude and phase weighting. Since the elements are equally spaced in the γ and ϕ directions,

$$\gamma_m = m\Delta\gamma\,, \tag{9.2-12}$$

where

$$\Delta\gamma = \frac{180^\circ}{M+1}\,, \tag{9.2-13}$$

and

$$\phi_n = (n-1)\Delta\phi\,, \tag{9.2-14}$$

where

$$\Delta\phi = 360^\circ/N\,. \tag{9.2-15}$$

Substituting (9.2-10) into (9.2-7) yields the following expression for the far-field beam pattern of a spherical array of identical, equally-spaced, complex-weighted, omnidirectional point-elements:

$$D(f,\theta,\psi) = \mathcal{S}(f)\sum_{m=1}^{M}\sum_{n=1}^{N} c_{mn}(f)\exp\left\{+j\frac{2\pi a}{\lambda}\left[\sin\gamma_m \sin\theta\cos(\psi-\phi_n)\right]\right\}\times \exp\left\{+j\frac{2\pi a}{\lambda}\cos\gamma_m\cos\theta\right\} \tag{9.2-16}$$

where $\mathcal{S}(f)$ is the complex, element sensitivity function, and the double summation is the dimensionless array factor. If one or more elements in the array are broken (not transmitting and/or receiving), set $c_{mn}(f) = 0$ for those elements. Similarly, if only one stave is in operation at any given instant of time, set $c_{mn}(f) = 0$ for those elements not in operation.

If the number of circular arrays $M = 1$, then $\Delta\gamma = 90^\circ$ [see (9.2-13)] and $m = 1$. And since $\gamma_1 = 90^\circ$ [see (9.2-12)], (9.2-16) reduces to

$$D(f,\theta,\psi) = \mathcal{S}(f)\sum_{n=1}^{N} c_n(f)\exp\left[+j\frac{2\pi a}{\lambda}\sin\theta\cos(\psi-\phi_n)\right]. \tag{9.2-17}$$

Equation (9.2-17) is the far-field beam pattern of a single circular array with radius a meters lying in the XY plane [see (8.1-92)].

Since

$$\cos(\psi - \phi_n) = \cos\psi\cos\phi_n + \sin\psi\sin\phi_n\,, \tag{9.2-18}$$

(9.2-16) can be rewritten as follows:

$$D(f,\theta,\psi) = \mathcal{S}(f)\sum_{m=1}^{M}\sum_{n=1}^{N} c_{mn}(f)\exp\left\{+j\frac{2\pi}{\lambda}\left[x_{mn}\sin\theta\cos\psi + y_{mn}\sin\theta\sin\psi\right]\right\}\times \exp\left\{+j\frac{2\pi}{\lambda}z_m\cos\theta\right\} \tag{9.2-19}$$

where

$$x_{mn} = a\sin\gamma_m\cos\phi_n\,, \tag{9.2-20}$$

$$y_{mn} = a\sin\gamma_m\sin\phi_n\,, \tag{9.2-21}$$

and

$$z_m = a\cos\gamma_m \tag{9.2-22}$$

are the rectangular coordinates of element (m,n), γ_m is given by (9.2-12), and ϕ_n is given by (9.2-14).

9.2.1 The Phased Array – Beam Steering

Beam steering can be accomplished by operating staves in a clockwise or counterclockwise fashion, analogous to the scanning procedure that was discussed for a cylindrical array in Subsection 9.1.1 (see Example 9.1-1). When a particular stave is in operation, the far-field beam pattern of the stave can be steered to $\theta = \theta'$ and $\psi = \psi'$ by using the following phase weights:

$$\theta_{mn}(f) = -\frac{2\pi}{\lambda}(x_{mn}\sin\theta'\cos\psi' + y_{mn}\sin\theta'\sin\psi' + z_m\cos\theta'), \qquad \begin{matrix} m = 1,2,\ldots,M \\ n = 1,2,\ldots,N \end{matrix} \tag{9.2-23}$$

where x_{mn}, y_{mn}, and z_m are given by (9.2-20) through (9.2-22), respectively. Substituting (9.2-11) and (9.2-23) into (9.2-19) yields

$$D(f,\theta,\psi)=\mathcal{S}(f)\sum_{m=1}^{M}\sum_{n=1}^{N}a_{mn}(f)\exp\left[+j\frac{2\pi}{\lambda}(\sin\theta\cos\psi-\sin\theta'\cos\psi')x_{mn}\right]\times$$
$$\exp\left[+j\frac{2\pi}{\lambda}(\sin\theta\sin\psi-\sin\theta'\sin\psi')y_{mn}\right]\times$$
$$\exp\left[+j\frac{2\pi}{\lambda}(\cos\theta-\cos\theta')z_{m}\right] \tag{9.2-24}$$

Set $a_{mn}(f)=0$ in (9.2-24) for those elements not in operation. As was previously mentioned in Subsection 9.1.1 for a cylindrical array, by operating two or more staves at the same time and using parallel signal processing, multiple beams with multiple "look directions" can be formed simultaneously.

The equivalent time delay τ'_{mn} in seconds at element (m,n) is given by [see (9.1-40)]

$$\tau'_{mn}=-\theta_{mn}(f)/(2\pi f). \tag{9.2-25}$$

Substituting (9.2-23) into (9.2-25) yields

$$\tau'_{mn}=\frac{u'}{c}x_{mn}+\frac{v'}{c}y_{mn}+\frac{w'}{c}z_{m}, \qquad \begin{matrix} m=1,2,\ldots,M \\ n=1,2,\ldots,N \end{matrix} \tag{9.2-26}$$

where $c=f\lambda$, and u', v', and w' are given by (9.1-43) through (9.1-45), respectively.

Problems

Section 9.1

9-1 Consider a linear array composed of an odd number M of identical, unevenly-spaced, complex-weighted, omnidirectional point-elements in three-dimensional space (see Fig. P9-1).

(a) Find the unnormalized, far-field beam pattern of this array as a function of frequency f and spherical angles θ and ψ. **Hint:** Generalize the results in Example 8.1-8.

(b) Find the equation for the phase weights that must be used in order to

do beam steering. **Hint:** Generalize the results in Example 8.2-1.

(c) Find the equation for the equivalent time delays. **Hint:** Generalize the results in Example 8.2-1.

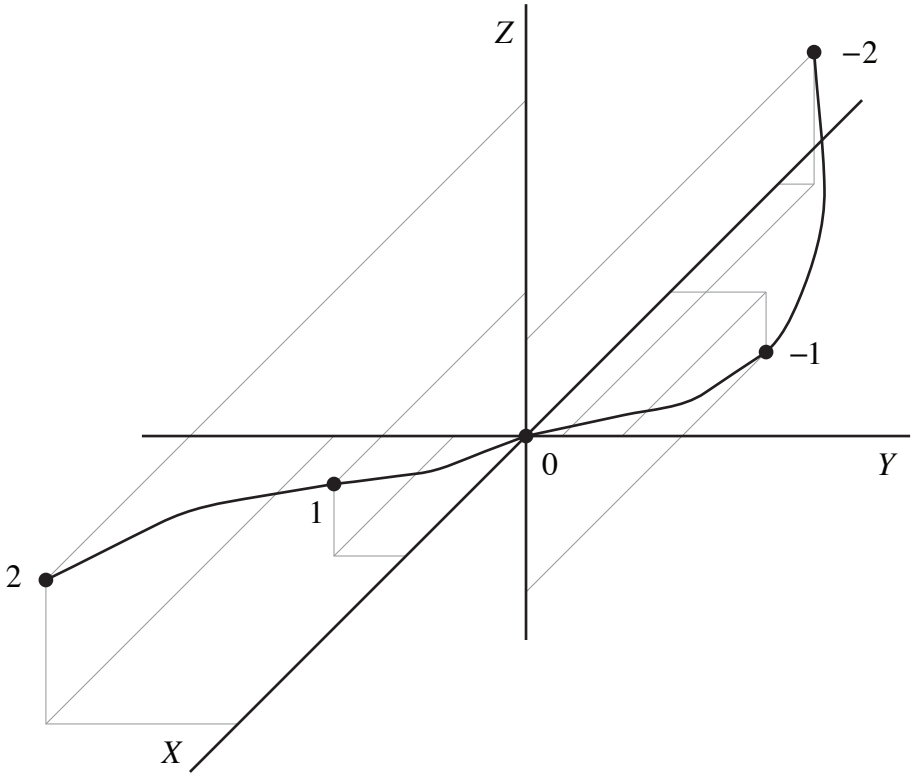

Figure P9-1

9-2 The arc length s in meters between two adjacent omnidirectional point-elements on a circular array on the surface of the cylinder shown in Fig. 9.1-2 is $s = a\Delta\phi$, where a is the radius of the cylinder in meters and $\Delta\phi$ is the angular spacing in *radians*.

(a) How many omnidirectional point-elements per circular array M must be used so that $s \le \lambda/2$?

(b) How many circular arrays N must be used so that the spacing $d_z \le \lambda/2$?

9-3 For the cylindrical array described in Example 9.1-1,

(a) find the magnitude of the normalized, horizontal, far-field beam pattern of stave 2 for rectangular amplitude weights and beam-steer